DOI: 10.13009/EUCASS2022-6040
9TH EUROPEAN CONFERENCE FOR AERONAUTICS AND SPACE SCIENCES (EUCASS)

A Revised Model of Ammonium Perchlorate Combustion with Detailed Kinetics

BERNIGAUD Pierre [1†], *DAVIDENKO Dmitry* [1], *CATOIRE Laurent*[2]
[1] *DMPE, ONERA, Université Paris Saclay, F-91120 Palaiseau, France*
[2] *Unité Chimie et Procédés (UCP), ENSTA Paris, Institut Polytechnique de Paris, 91120 Palaiseau, France*
pierre.bernigaud@onera.fr · dmitry.davidenko@onera.fr · laurent.catoire@ensta-paris.fr
[†]Corresponding author

Abstract

In this study, we propose a revised detailed kinetic model for ammonium perchlorate (AP) combustion, leveraging recent advances in the modelling of ammonia chemistry. The gas-phase mechanism is validated against data on species sampling in jet-stirred reactors, laminar flame speed measurements, and ignition delay time. A new model of AP decomposition in the condensed phase is proposed to be used with the gas-phase mechanism. The AP laminar flame is then simulated in the 1D coupled approach. These calculations provide results on the regression rate, surface temperature, temperature sensitivity and species profiles for a prescribed initial temperature of AP and ambient pressure. Stability analysis of the coupled model is carried out employing the Zel'dovich-Novozhilov method.

1. Introduction

Ammonium perchlorate (AP), combined with a polymeric binder such as hydroxytelechelic polybutadiene (HTPB), is a widely used ingredient for composite solid propellants. These composite propellants are used for both civilian and military applications. While the binder provides the combustible gases via its pyrolysis, the AP acts as a source of oxidant. The combustion process is then controlled by the modal distribution of the AP particles in the propellant. The composite propellant can be tailored to meet specific requirements using appropriate AP loading.
In order to design a composite propellant, it is important to understand and properly model the combustion of pure AP. To this end, it is necessary to develop a detailed chemical kinetic mechanism in the gas phase and a model of the AP decomposition processes in the condensed phase. Extensive experimental work has been carried out in the past, the results of which are essential for the construction and validation of numerical models. The models must first verify the macroscopic characteristics of the AP combustion: Atwood and Boggs [1] measured the regression rate of AP at various pressures, as well as the initial temperature sensitivity. Surface temperature measurements were performed by Bakhman [2], Powling [3] as well as Korobeinichev [4]. The combustion model must also represent the underlying chemical mechanisms within the flame. To this end, the work of Ermolin [5] provides chemical species profiles in an AP flame at low pressure. For this same flame, Tereshenko [6] reports measurements of the temperature profile near the regression surface. On this experimental base, Ermolin [5] proposed a first chemical kinetics mechanism in the gas phase, able to reproduce satisfactorily the measured species profiles. Tanaka [7] then Jing [8] presented models coupling the gas-phase combustion and condensed-phase decomposition processes. The inclusion of the condensed phase has improved the macroscopic performance of the model (prediction of burning rate, temperature sensitivity). Efforts to develop more accurate detailed kinetic models for the combustion of ammonium perchlorate were continued by Meynet [9], Gross [10] and Smyth [11]. Ammonium perchlorate (NH_3HClO_4) decomposes in the condensed phase via different pathways, the most important of them forming NH_3 and $HClO_4$. The presence of NH_3 among the main decomposition products requires an appropriate kinetic model for NH_3, its subsequent radicals, and NO_x. Chemical experiments involving ammonia have been numerically reproduced with the model used by Gross [10], highlighting some important deficiencies. Based on this finding, we first propose a new gas-phase kinetic model for AP combustion based on Shrestha's recent work on ammonia oxidation [12]. A revised model of the condensed phase decomposition process is then formulated to be coupled to the new gas-phase kinetic mechanism. Simulations of AP combustion using a coupled flame/solid approach are performed to evaluate the macroscopic parameters (burning rate, surface temperature), serving as validation criteria with respect to the available experimental data. Temperature and chemical species profiles are computed for the low-pressure flame studied by Ermolin [5] and Tereshenko [6]. Finally, a stability study is carried out, in the sense of the Zel'dovich-Novozhilov theory [13].

DOI: 10.13009/EUCASS2022-6040

2. Gas Phase Mechanism

The proposed mechanism for AP combustion consists of 36 species and 205 reactions. It is composed of an O-H sub-mechanism, a sub-mechanism for nitrogen-containing species, and a sub-mechanism for chlorinated species. This model was developed based on the work of Shrestha [12] on ammonia combustion for the H-O-N part of the mechanism. The sub-mechanism for chlorinated species is inspired by the work of Smooke and Yetter [14], itself based on the mechanism proposed by Ermolin [15]. This last sub-mechanism also includes reactions used by Pelucchi [16] in his study of HCl/Cl_2 chemistry at high temperature.
The ability of the mechanism to accurately represent the NH_3 chemistry is first validated via laminar flame speed and ignition delay calculations. The H_2/NO_x sub-mechanism is tested on experiments in a jet-stirred reactor. The correct treatment of the Cl_2 chemistry is also verified via laminar flame speed and ignition delay calculations. The new mechanism is compared to the reference model of Gross [10] (25 species, 80 reactions).

2.1 NH_3 Chemistry

Ammonia (NH_3) is one of the main decomposition products of ammonium perchlorate. In order to validate the oxidation sub-mechanism of NH_3, different experiments are reproduced with the new model. The ignition delay time for a highly diluted NH_3/O_2 mixture is calculated for various pressure and equivalence ratio. The results are compared in Figure 2 with the measurements in shock tube experiments by Mathieu [17].

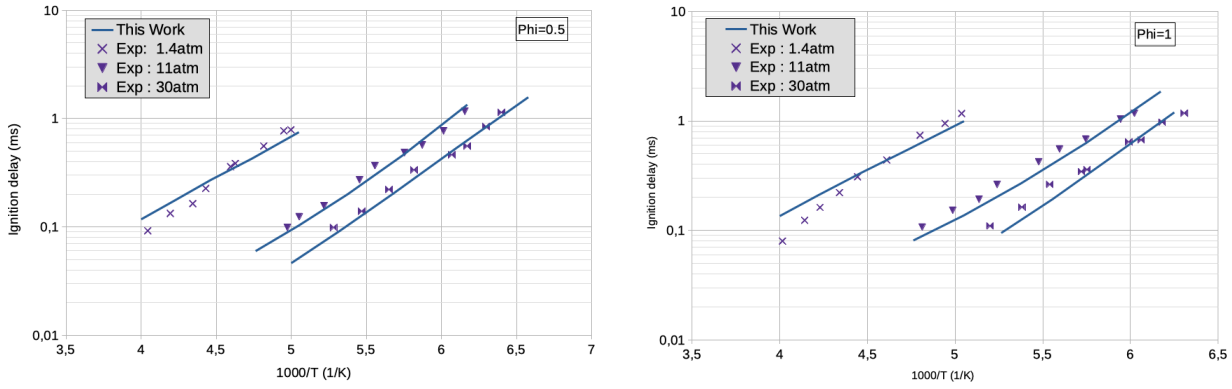

Figure 1: Ignition delay time for NH_3/O_2 mixtures for various pressure (1.4, 11 and 30 atm) and equivalence ratio (ϕ = 0.5 and 1). Symbols: experiment [17]. Lines: model predictions.

A good agreement between the model predictions and experimental results is achieved. The results obtained with the Gross model [10] are not reported because no ignition was observed with this mechanism. Indeed, this model has neither reaction between NH_3 and O_2, nor dissociation reaction for NH_3. The ignition is initiated in the present mechanism via the following reactions:

$$NH_3 + M = NH_2 + H + M \quad (1)$$

$$NH_3 + O_2 = HO_2 + NH_2 \quad (2)$$

The second reaction is particularly important. It produces hydrogen atoms, which participate in the formation of the OH and O radicals via the reaction:

$$H + O_2 = OH + O \quad (3)$$

The consumption of ammonia NH_3 is then controlled mainly by the reactions with the H, O and OH radicals.
The predicted laminar flame velocities for the NH_3/air system at 1 atm are presented in Figure 2 and compared with available experimental data. Also reported are the predictions with the models of Gross [10] and Shrestha [12] that served as the basis for the development of the present model.
We observe a good agreement between the predictions of the present model and the experimental results. The Gross model [10] overpredicts the flame speed, especially at lower equivalence ratios but captures the velocity maximum around stoichiometry. It may be noted that the present mechanism appears to perform slightly better than the Shrestha model [12] for rich conditions, where the slope drawn by the experimental points is well followed.

DOI: 10.13009/EUCASS2022-6040

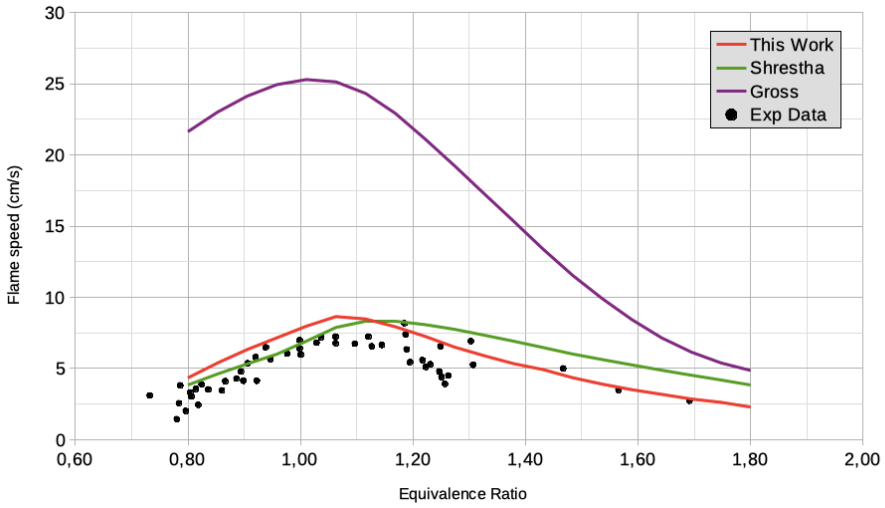

Figure 2: Laminar flame speed versus equivalence ratio for NH_3/air mixtures at 1 atm and 298 K. Symbols: experiments [18–23]. Lines: Models predictions.

2.2 H_2 and NO_x Chemistry

The combustion of ammonium perchlorate produces various NO_x species. It is therefore important to ensure the validity of the NO_x sub-mechanism. The NO_x and H_2 oxidation sub-mechanisms are validated on experiments in jet-stirred reactor. The first test case, Figure 3, corresponds to the reaction products of a H_2 (1%) / O_2 (1%) / N_2 mixture doped with 220 ppm of NO. The pressure is 10 atm and the residence time is 1s.

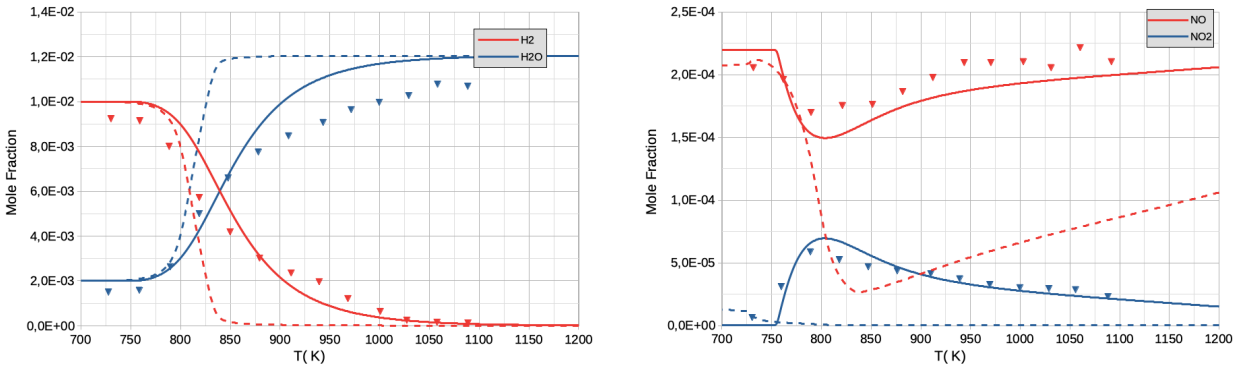

Figure 3: Reaction products of the mixture H_2 (1%) / O_2 (1%) / N_2 doped by 220 ppm of NO in a jet-stirred reactor at 10 atm, residence time 1s, variable temperature. Symbols: experiment [24]. Solid lines: present model. Dashed lines: Gross model

.

The Gross model [10] correctly predicts the intersection of the H_2 and H_2O curves, around 825 K, but the results deviate rapidly from the experimental points as the temperature increases. The present model shows a satisfactory behavior. The reaction is initiated by:

$$H_2 + O_2 = HO_2 + H \tag{4}$$

H_2 is then converted into H_2O via:

$$OH + H_2 = H_2O + H \tag{5}$$

DOI: 10.13009/EUCASS2022-6040

The rate of consumption of H_2 is therefore controlled by the OH concentration in the gas. Three pathways for the production of OH are identified:

$$H + O_2 = O + OH \quad (6)$$
$$NO_2 + H = NO + OH \quad (7)$$
$$NO + HO_2 = NO_2 + OH \quad (8)$$

At low temperature (700 K), these three reactions are not very active, prohibiting the conversion of H_2 to H_2O. At 850 K, the third pathway is particularly active: we observe a conversion from NO to NO_2 and an acceleration of the hydrogen chemistry. At higher temperatures, the first and second pathways are more active, reforming NO from NO_2. In the Gross mechanism, the third pathway is absent, which explains why the NO to NO_2 conversion is not observed. At 850 K, the first and second pathways are very active: OH is produced in large quantities, and the oxidation of H_2 is overly accelerated. The drop in the level of NO is explained by its conversion via HNO into NO_2, which is instantaneously transformed into OH via the second pathway to accelerate the H_2 oxidation.

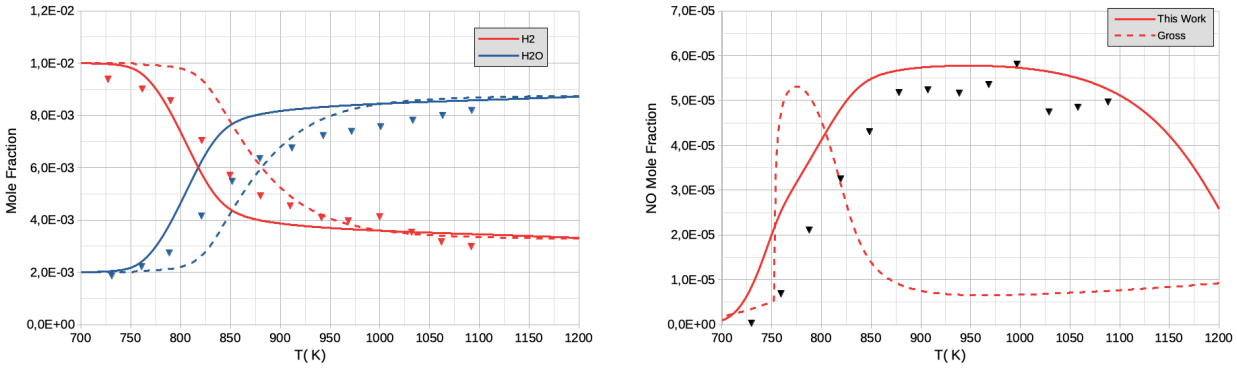

Figure 4: Reaction products of a H_2 (1%) / O_2 (0.333%) / N_2 mixture doped by 60 ppm of NO_2 in a jet-stirred reactor at 10 atm, 1s residence time, variable temperature. Symbols: experiment [24]. Solid lines: present model. Dashed lines: Gross model [10].

Another case studied is presented in Figure 4, the reaction in a jet-stirred reactor of a mixture H_2 (1%) / O_2 (0.333%) / N_2 doped by 60 ppm of NO_2 at 10 atm. For both models the conversion H_2 to H_2O is predicted satisfactorily, the conversion NO_2 to NO takes place via the second pathway. This reaction is proceeding too rapidly in the Gross model, causing an overproduction of NO at low temperature. NO formed is then rapidly converted into N_2 in the Gross mechanism via the reaction NO + HNO = N_2 + HO_2 which is responsible for the low NO level at high temperature. This last reaction is absent in the new model.

2.3 Cl_2 Chemistry

The sub-mechanism representing the chemistry of chlorinated species is also validated in comparison with experimental data on the ignition delay and laminar flame speed for the Cl_2 / H_2 system.
The results on the ignition delay time for different $Cl_2/H_2/Ar$ mixtures are reported in Figure 5. The experimental points come from measurements made by Lifshitz and Schechner [25] in a shock tube over the temperature range 830-1260 K. The different experimental cases considered are specified in Table 1. The mole fractions represent the reactant composition , P_1 is the initial pressure in the shock tube, and P_5 is the pressure after the reflected shock.

Table 1: Experimental cases considered for the ignition simulations of $Cl_2/H_2/Ar$ mixtures

Case	Cl_2 (%)	H_2 (%)	P_1 (atm)	P_5 (atm)
A	10.4	10.4	0.066	1.0
B	10.4	10.4	0.263	4.6
C	19.8	10.0	0.066	1.3
D	10.3	21.6	0.066	1.3
E	11.0	11.0	0.066	1.3

DOI: 10.13009/EUCASS2022-6040

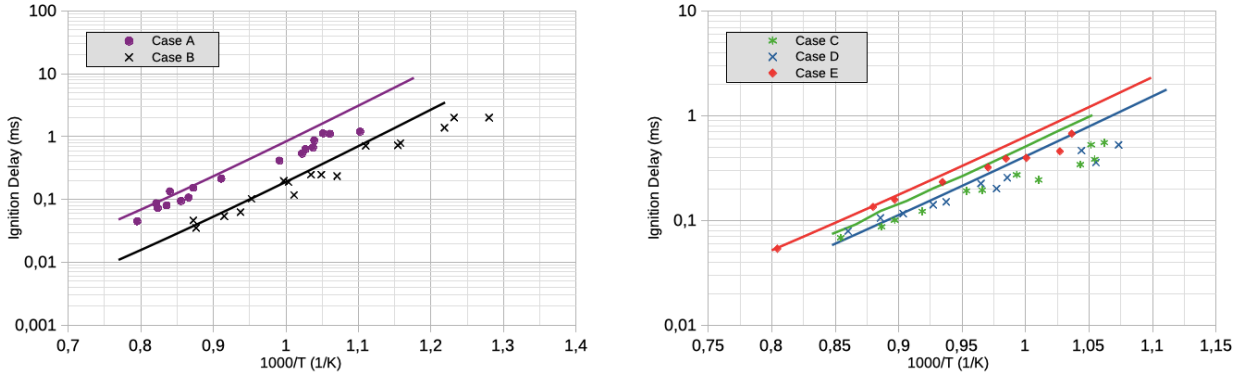

Figure 5: Ignition delay time for $Cl_2/H_2/Ar$ mixtures. Symbols: experiment [25]. Lines: model predictions.

Cases A and B are reproduced satisfactorily, demonstrating the ability of the model to represent the effect of pressure on the ignition delay for a stoichiometric mixture. Cases C, D, and E are performed at the same pressure for different equivalence ratios. Good agreement between the model and experimental points is observed for these cases at high temperatures. However, the predictions deviate from the experimental trend for lower temperatures, particularly in cases C and E. As reported by Pelucchi [16], the ignition delay is mainly controlled by the following reactions forming H radicals:

$$Cl_2 + M = Cl + Cl + M \quad (9)$$

$$Cl + H_2 = HCl + H \quad (10)$$

A more detailed analysis of the reaction kinetics could allow an improvement of the model predictions. However, the good performance observed at high temperatures remains satisfactory in modelling the combustion of ammonium perchlorate.

The sub-mechanism of chlorinated species is further validated by comparing the results on the laminar flame speed for Cl_2 / H_2 / N_2 mixtures with different dilution levels, Figure 6. A good agreement is found between the experimental points and the predictions obtained with the present model. For the Gross model, the laminar flame speed is systematically underestimated. This defect increases for more concentrated mixtures.

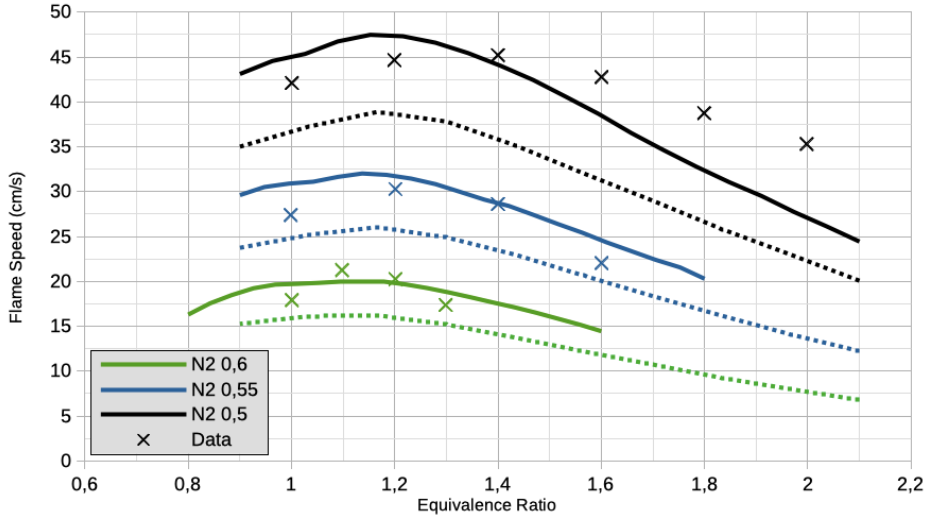

Figure 6: Laminar flame speed for $Cl_2/H_2/N_2$ mixtures at 1 atm, 298 K, and different mole fractions of N_2. Symbols: experiment [26]. Solid lines: present model. Dashed lines: Gross model [10].

DOI: 10.13009/EUCASS2022-6040

3. Coupled Combustion Model

The new gas-phase kinetic mechanism is applied to the case of ammonium perchlorate combustion. The calculations are performed in a coupled approach with the condensed phase. The gas and condensed phases are considered to be separated by a planar and infinitely thin interface for which the appropriate coupling conditions are formulated. The combustion process is assumed to be one-dimensional and steady-state.

3.1 Governing Equations

3.1.1 Gas Phase

For the gas phase, the governing equations for a reactive flow are formulated under the assumption of low Mach number. The continuity equation is expressed as:

$$\frac{\mathrm{d}}{\mathrm{d}x}\left(\rho_g u\right) = 0 \tag{11}$$

Where ρ_g is the bulk density of the gas and u is the flame speed. We then introduce the mass flux $m = \rho_g u$, constant in space. Under the adopted assumptions, the velocity is entirely defined by the continuity equation. The momentum equation allows obtaining the variation of the hydrodynamic pressure, which is not of interest to this problem. It is therefore not solved. The equation for the mass fraction Y_k of chemical species $k \in [\![1, N_s]\!]$ is :

$$m\frac{\mathrm{d}Y_k}{\mathrm{d}x} = -\frac{\mathrm{d}}{\mathrm{d}x}\left(\rho_g Y_k V_k\right) + \mathcal{M}_k \dot{\omega}_k \tag{12}$$

With $\mathcal{M}_k$ the molar mass of species k, $\dot{\omega}_k$ its molar production rate and V_k its diffusion velocity. Finally, the energy equation is expressed as:

$$\begin{cases} m\dfrac{\mathrm{d}h_g}{\mathrm{d}x} = \dfrac{\mathrm{d}Q_g}{\mathrm{d}x} \\ Q_g = \lambda_g \dfrac{\mathrm{d}T}{\mathrm{d}x} - \rho_g \displaystyle\sum_{k=1}^{N_s} h_k Y_k V_k \end{cases} \tag{13}$$

Where T is the temperature, h_g is the enthalpy of the gas, λ_g is its thermal conductivity, and h_k is the enthalpy of chemical species k.
These equations are discretized by the finite volume method and solved by a Newton-Raphson method. In order to facilitate the convergence, temporal terms are introduced and discretized using the backward Euler scheme. The gradients are assumed to be zero at the outlet boundary, and the inlet conditions are determined by the coupling equations with the condensed phase. The CHEMKIN library [27] is used for computing the reaction rates and thermodynamic properties in the gas phase. Transport properties (thermal conductivity, diffusion coefficients) are evaluated employing the EGLib library [28, 29].

3.1.2 Condensed Phase

By analogy with the gas-phase, the mass flux in the condensed phase is $m = \rho_c u$, where ρ_c is the corresponding density. The energy equation is:

$$\begin{cases} m\dfrac{\mathrm{d}h_c}{\mathrm{d}x} = \dfrac{\mathrm{d}Q_c}{\mathrm{d}x} \\ Q_c = \lambda_c \dfrac{\mathrm{d}T}{\mathrm{d}x} \end{cases} \tag{14}$$

Where are defined for the condensed phase the enthalpy h_c, and the thermal conductivity λ_c. This equation can be expressed as two ordinary differential equations:

$$\begin{cases} \dfrac{\mathrm{d}T}{\mathrm{d}x} = \nabla T \\ \dfrac{\mathrm{d}}{\mathrm{d}x}\left(\lambda_c \nabla T\right) = m c_c \nabla T \end{cases} \tag{15}$$

With c_c the heat capacity of the condensed phase. These equations are integrated using the DASSL algorithm [30], from the initial conditions:

DOI: 10.13009/EUCASS2022-6040

$$\begin{cases} T\left(x_{\text{ini}}\right) = T_{\text{ini}} \\ \left(\lambda_c T\right)_{\text{ini}} = m\left[h_c\left(T_{\text{ini}}\right) - h_c\left(T_0\right)\right] \end{cases} \tag{16}$$

With T_0 the initial temperature of the AP. The thermophysical properties of the AP are defined as dependent on the temperature and its physical state. Table 2 presents the model parameters for the solid and liquid phases. The transition enthalpy from the solid to liquid phase accounts for the transition enthalpy from the orthorhombic to cubic crystalline phase of AP.

Table 2: Thermophysical properties of AP

Property	**Solid AP**	**Liquid AP**	**Ref**
Density (kg/m^3)	1957	1756	[7]
Enthalpy at 298.15K (J/kg)	-2517423	-	[31]
Melting Temperature (K)	735	-	[11]
Transition Enthalpy (J/kg)	-	338312	[31], [7]
Thermal Capacity (J/kg/K)	$584.35 + 1.7054T$	1913	[32], [11]
Thermal Conductivity (W/m/K)	$0.64279 - 3.8493 \cdot 10^{-4}T$	$0.41631 - 1.5690 \cdot 10^{-4}T$	[32], [11]

3.2 Interface Conditions

The interface between the condensed AP and the gas phase is a difficult zone to model, owing to the complexity of the physical phenomena involved. A chemically reactive foam is found in this zone. The mass and heat transfer is accompanied by decomposition reactions in the condensed phase. Few experimental results are available to model these mechanisms. The study of this interface is also difficult due to its small thickness: Boggs [33] reports a thickness of 1 to 5 μm, while Tanaka and Beckstead [7] estimate a thickness of less than 1 μm. It is proposed for the present modeling approach to consider this area as an infinitely thin surface with appropriate conditions that are part of the present model. These conditions must ensure the transfer of mass, heat and species between the two phases while representing the chemical reactions taking place in the foam in a global sens.

3.2.1 Interface Chemistry

The AP decomposition is represented by surface reactions. It is commonly assumed [10, 34, 35], that AP decomposes via two competing paths. The first path is endothermic and results from direct sublimation of the AP via proton transfer and desorption:

$$\text{AP} \rightarrow \text{NH}_3 + \text{HCLO}_4 \tag{17}$$

The second exothermic path, forming N chemical species and hereafter called the decomposition path, is meant to model the remaining chemical reactions:

$$\text{AP} \rightarrow \sum_{k=1}^{N} \nu_k \chi_k \tag{18}$$

Where χ_k designates the k-th product species and ν_k its stoichiometric coefficient. Numerous variants have been proposed for this pathway by several authors [7, 10, 11]. These models produce unsatisfactory results when coupled with the gas-phase reaction mechanism presented above. A new decomposition reaction is therefore proposed to be used in conjunction with the gas-phase mechanism:

$$\text{AP} \rightarrow \frac{7}{26}\text{N}_2 + \frac{23}{26}\text{O}_2 + \frac{46}{26}\text{H}_2\text{O} + \frac{7}{26}\text{Cl}_2 + \frac{12}{26}\text{HCl} + \frac{4}{26}\text{NO}_2 + \frac{4}{26}\text{N}_2\text{O} \tag{19}$$

The relative importance of the two paths is controlled by parameter α, such that the global reaction resulting from the two paths considered can be written as:

$$\text{AP} \rightarrow \alpha\left(\text{NH}_3 + \text{HCLO}_4\right) + (1-\alpha)\sum_{k=1}^{N} \nu_k \chi_k = \sum_{k=1}^{\hat{N}} \hat{\nu}_k \chi_k \tag{20}$$

DOI: 10.13009/EUCASS2022-6040

Where we introduce $\hat{\nu}_k$ the stoichiometric coefficient of species k in the global reaction including both paths. Since the sublimation and decomposition paths are respectively endothermic and exothermic, this α parameter has a first-order effect on the regression rate predicted by the present model: the mass flow rate increases as the value of α decreases. It is assumed in this study that α is independent of the ambient pressure and initial temperature of AP. It is fixed at a value of 0.65 to reproduce the experimentally observed evolution of the regression rate as a function of the pressure. The regression mass flux m depends on the molar consumption rate of AP at the interface, $\hat{\omega}_{\mathrm{AP}}$. This rate is related to the surface temperature via a pyrolysis law, Equation (21). Its parameters are grouped in Table 3.

$$m = -\mathcal{M}_{\mathrm{AP}}\hat{\omega}_{\mathrm{AP}} = A \exp\left(\frac{-T_a}{T_s}\right) \tag{21}$$

Table 3: Parameters for the AP pyrolysis law

Parameter	**Value**
Molar mass (kg/mol)	0.11748
Ta (K)	7400
A (kg/m^2/s)	$1.5 \cdot 10^4$

3.2.2 Flux Conservation

We introduce x_s the position of the interface and the notation $[\,\cdot\,]$ such that:

$$[X] = X_g^I - X_c^I \tag{22}$$

Where $X_c^I = X_c(x = x_s)$ and $X_g^I = X_g(x = x_s)$ are quantities representing the boundary conditions at the interface for each phase. The interface is infinitely thin and is assumed to contain no source of mass or energy. The conservation of mass and energy fluxes across the interface leads to:

$$[m] = [\rho u] = 0 \tag{23}$$

$$[mh - Q] = 0 \tag{24}$$

The mass flux of species k in the gas phase is expressed at the interface as:

$$mY_k^I + \left(\rho_g Y_k V_k\right)^I = -\mathcal{M}_k \hat{\nu}_k \hat{\omega}_{\mathrm{AP}} \tag{25}$$

We also impose the continuity of the temperature profile:

$$T_g^I = T_c^I = T_s \tag{26}$$

3.3 Solution Method for the Coupled Problem

Two one-dimensional physical domains are considered, for the condensed and gaseous phase. In order to ensure a correct coupling, a global iterative algorithm is employed to find the mass flow verifying the interface conditions. The residual defined by Equation (24) must disappear through these iterations. At each global iteration, the solution in the condensed phase is obtained for the imposed mass flux by integrating Equation (15). The solution for the flame is obtained with the surface temperature, for which the imposed mass flux corresponds to the surface regression rate defined by the pyrolysis law, Equation (21). The temperature profile in the condensed phase is interpolated at the surface temperature to obtain the interface conditions on the condensed phase side. The interface conditions for the gas phase are obtained via Equations (26) and (25). The mesh of the gas phase domain is automatically refined to limit the relative variation of variables between two cells and the relative variation of solution variable differences between three adjacent cells.

DOI: 10.13009/EUCASS2022-6040

4. AP combustion results

4.1 Ermolin's Flame

The coupled approach described above is first applied to the case of the low-pressure AP flame studied by Ermolin [5] and Tereshenko [6]. The mole fraction profiles obtained with the flame model, in comparison with the experimental points, for the main AP flame products as well as for nitrogen containing species are presented in Figure 7. We observe that the profiles are well reproduced by the model.

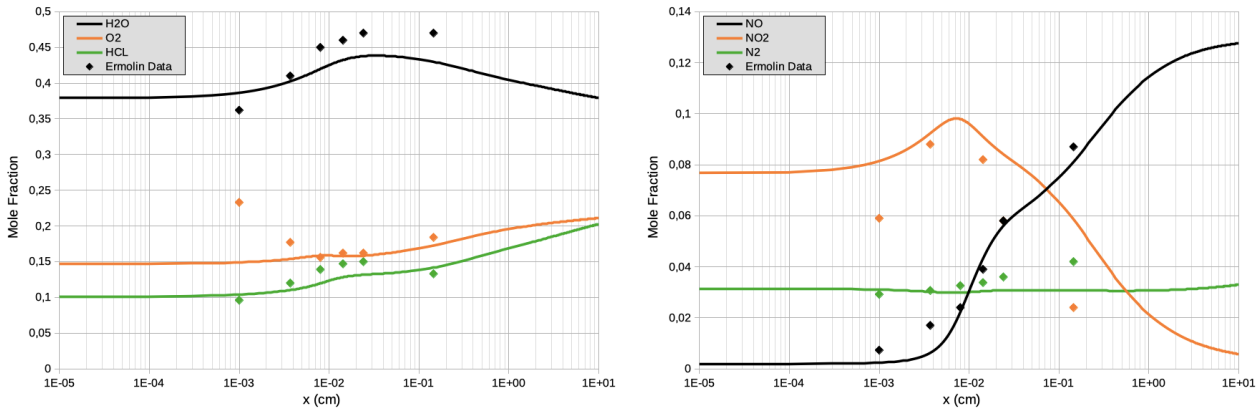

(a) Main products

(b) Main nitrogen containing species

Figure 7: Species profiles for the AP flame at 0.6 atm and initial temperature 533 K. Symbols: experiment [5]. Lines: model prediction.

The results obtained with the present model and the models of Smyth [11] and Meynet [9] are compared. The temperature profiles obtained for these different models are plotted in Figure 8 .

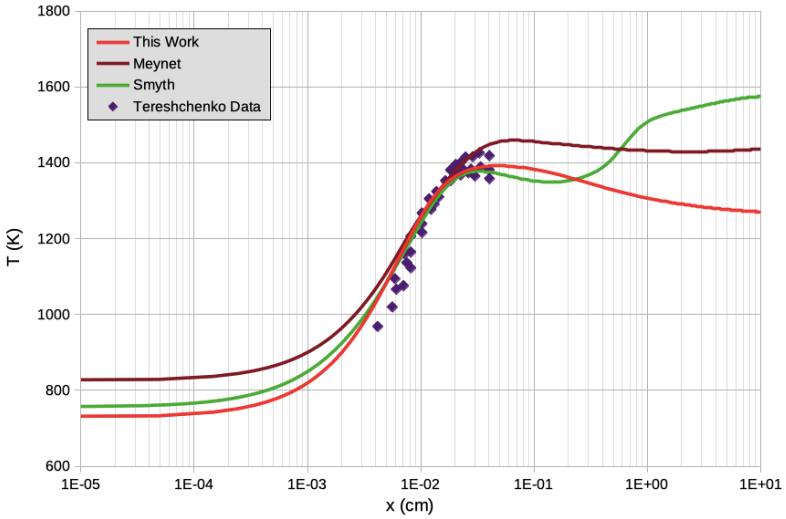

Figure 8: Temperature profiles in the AP flame at 0.6 atm and initial temperature 533 K. Symbols: experiment [6]. Lines: model prediction.

It is observed that the present model produces a profile in good agreement with the experimental points. The other reference models show satisfactory curves when compared to the experiment. The three models differ mainly in the predicted surface temperature and the downstream behaviour. The Smyth model is particularly distinguished by a second marked rise in temperature. This phenomenon can be explained by studying the NO and N_2 profiles predicted by the different models, Figure 9.

DOI: 10.13009/EUCASS2022-6040

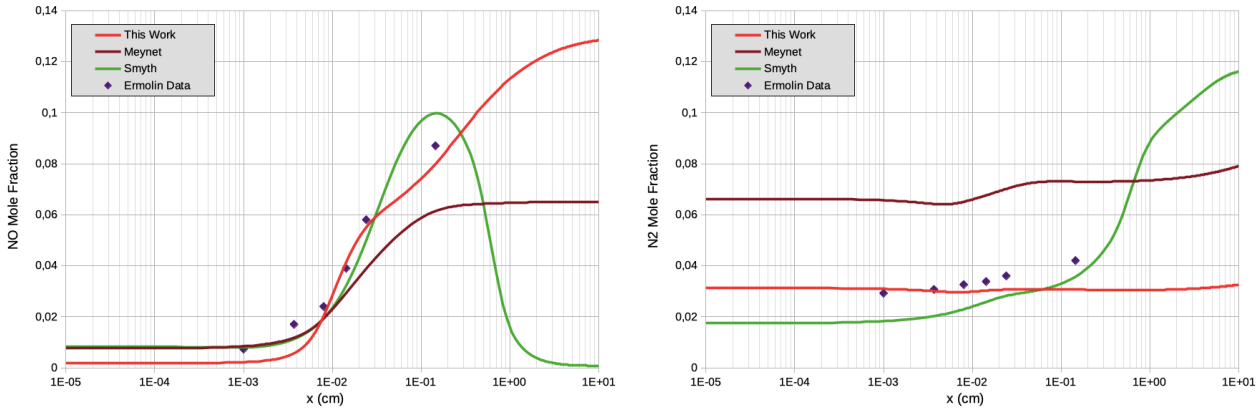

(a) NO Mole Fraction

(b) N_2 Mole Fraction

Figure 9: Profiles of NO and N_2 in the AP flame at 0.6 atm and initial temperature 533. Symbols: experiment [5]. Lines: model prediction.

We observe a very quick conversion of NO produced in the flame into N_2 via the irreversible reaction $2NO \rightarrow N_2 + O_2$ in the Smyth model. The second temperature rise observed with the Smyth model is caused by the energy released by this specific reaction. This reaction was introduced in order to decrease the NO level in the tail of the flame, judged by Smyth to be too far from the thermochemical equilibrium. Such an irreversible and non-elemental reaction appears to be artificial and destabilizes the equilibrium of the NO_x chemistry. The proposed model, whose NO_x chemistry has been previously validated on experimental cases, predicts a significant level of NO and reproduces the experimental points of [5]. These results suggest that NO may be an important end product for the AP flame: thermochemical equilibrium may be reached far downstream of the flame.

4.2 Macroscopic Parameters

The validity of the coupled model is further verified by analyzing the macroscopic parameters of the AP combustion. The evolution of the regression rate of AP with pressure is presented in Figure 10.

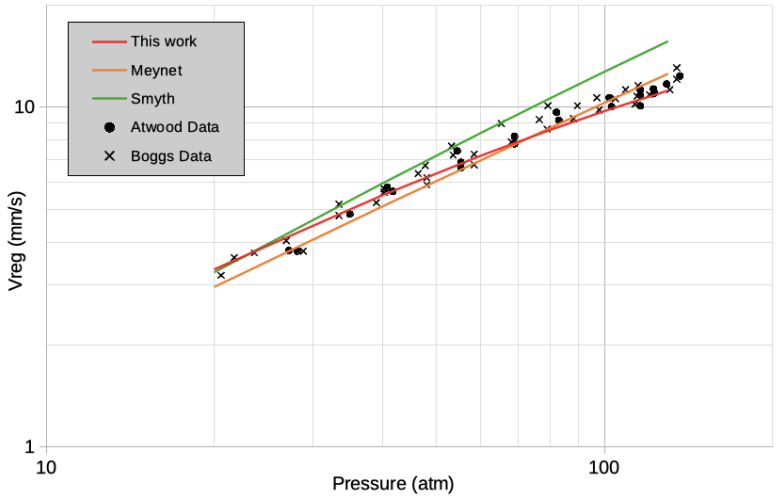

Figure 10: AP regression rate as a function of pressure. Initial temperature 298 K. Symbols: experiments [1, 33]. Lines: model predictions.

We observe a good agreement between the experimental points and the model predictions. The curves obtained for the different models can be approximated by a Vieille law of the form:

$$V_{\text{reg}} = aP^n \tag{27}$$

DOI: 10.13009/EUCASS2022-6040

Where V_{reg} is the regression speed and P the ambient pressure. We note that n is independent of pressure for the models of Meynet and Smyth. In the case of the present model, n decreases with pressure. This behaviour is consistent with the experimental results: the AP regression rate increase slows down at high pressure. Thus, while the Smyth model predicts the same regression rate as the present model for a pressure of 20 atm, it tends to overestimate the regression rate at pressures higher than 80 atm.

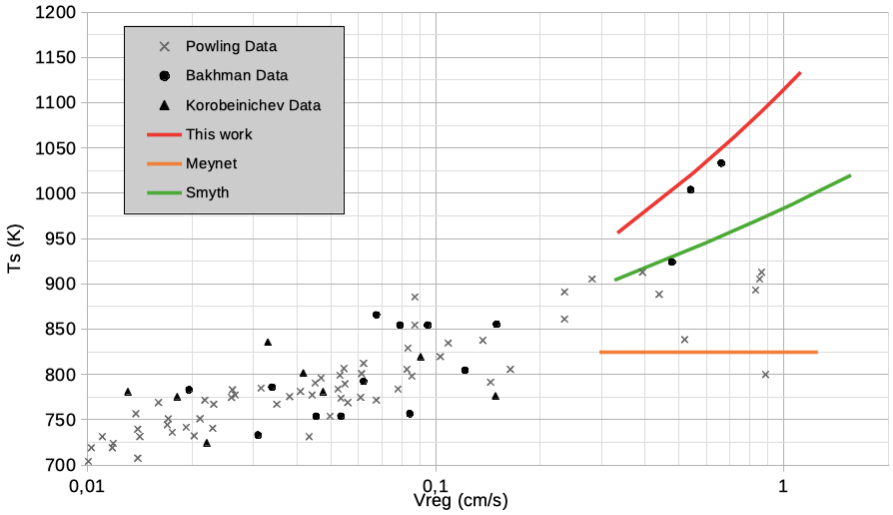

Figure 11: AP surface temperature as a function of regression rate. Initial temperature 298 K. Symbols: experiments [2–4]. Lines: model prediction.

The evolution of the AP surface temperature with the regression rate is shown in Figure 11. The Meynet model assumes the surface temperature to be independent of the regression rate and equal to the melting temperature of AP (850 K in this model). This assumption appears to be too simplifying in view of the higher surface temperatures experimentally observed. The curve produced by the present model is above the Smyth model curve, but still indicates acceptable temperatures considering the large scatter in the experimental data in this range of regression rates. It can be noted that this dependence is almost entirely controlled by the parameters of the pyrolysis law.

4.3 Stability Study

The combustion of ammonium perchlorate can be unstable under certain conditions, independently of external acoustic disturbances. This is the so-called intrinsic combustion instability of the propellant. These phenomena were studied by Denison and Baum [36], then by Zel'dovich and Novozhilov [13]. The two studies, following different reasoning, result in the same stability limit. According to the Zel'dovich-Novozhilov theory, this limit is characterized by sensitivity parameters from the steady-state combustion of the propellant. We define these parameters at constant pressure:

$$k = (T_s - T_0)\left(\frac{\partial \ln m}{\partial T_0}\right)_P \tag{28}$$

$$r = \left(\frac{\partial T_s}{\partial T_0}\right)_P \tag{29}$$

Where k and r are the sensitivity coefficients of the mass flux and the surface temperature to the initial propellant temperature T_0. By introducing a small perturbation of the regression velocity and temperature field in the condensed phase and then linearizing the energy equation in the propellant, it is possible to obtain the stability condition:

$$r > r_L = \frac{(k-1)^2}{k+1} \tag{30}$$

The parameters k and r have been calculated at different pressures for the present model and the Smyth model. Both models are stable at low pressure and approach the stability limit as the pressure increases. In order to characterize more precisely the stability limit of the two models, the evolution of r and r_L with pressure is plotted in Figure 12. The

DOI: 10.13009/EUCASS2022-6040

combustion becomes unstable at the crossing point of these two curves, following an oscillatory regime. The Smyth model becomes unstable around 8.75 MPa, while the present model is stable up to 11 MPa. This increased stability range is of practical interest, allowing unsteady calculations to be performed over a broader range of pressure.

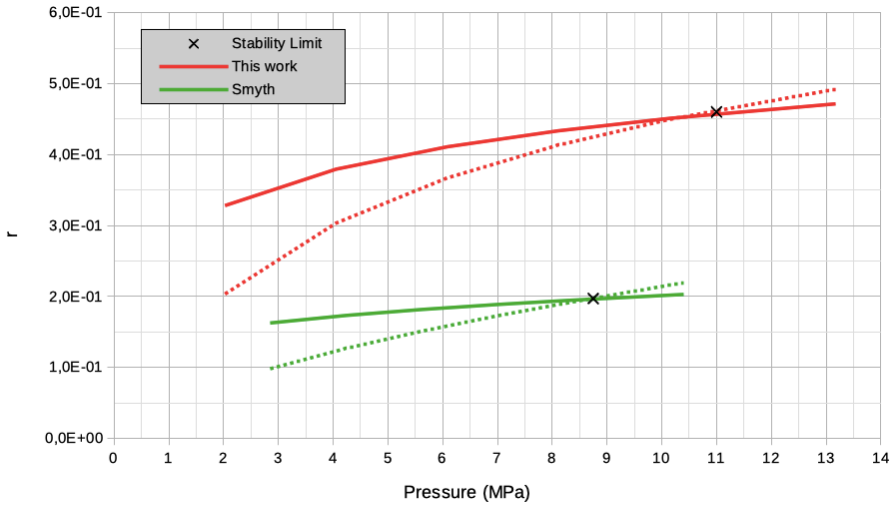

Figure 12: Stability limit according to the Zel'dovich-Novozhilov theory for different models. r (solid lines) and r_L (dotted lines).

We also define the temperature sensitivity coefficient of the propellant:

$$\sigma = \left(\frac{\partial \ln V_{\text{reg}}}{\partial T_0} \right)_P = \frac{k}{(T_s - T_0)} \tag{31}$$

The trends $\sigma(P)$ for the different models considered are reported in Figure 13. These results are compared to the experimental data of Atwood [1]. It is observed that the experimental trend is not captured by the models, as they predict a constant temperature sensitivity over the studied pressure range. The present model predictions are in satisfactory agreement with the experimental points, considering their important dispersion. We can note that the parameters r and σ largely depend on the pyrolysis law parameters. Indeed, increasing the pre-exponential coefficient A and decreasing the activation temperature T_a helps to stabilize the combustion.

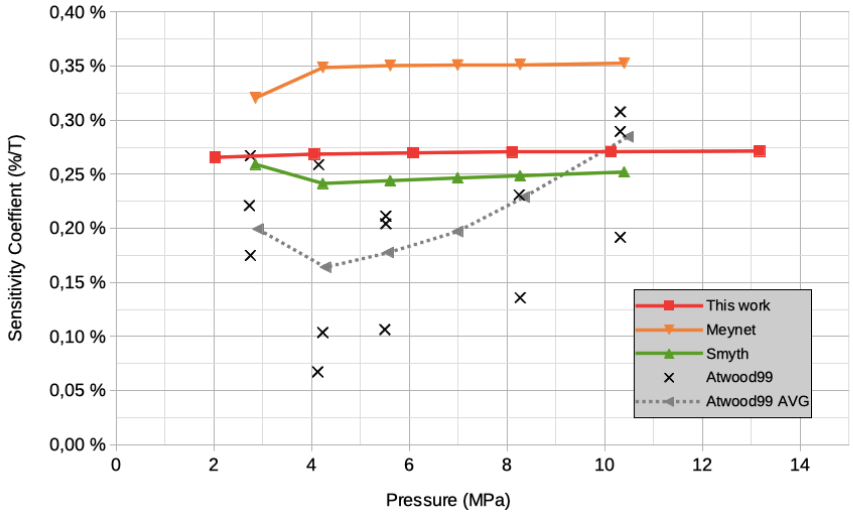

Figure 13: Temperature sensitivity as a function of pressure. Symbols: experiment [1]. Lines: models

DOI: 10.13009/EUCASS2022-6040

5. Conclusion

Using recent results from Shrestha [12] and Pelucchi [16], a revised gas-phase mechanism for AP combustion has been elaborated. This new mechanism produces satisfactory results for simple reactive systems, allowing validation of its $O - H$, NH_3, NO_x, and Cl_2 sub mechanisms. The test cases also revealed deficiencies in the Gross reference model [10]. The main deficiencies observed are an overestimation of the laminar flame speed for the NH_3 / air mixture, the absence of an initiation reaction for the ignition of a NH_3/O_2 mixture, an imbalance of the NO/NO_2 system, as well as an underestimation of the laminar flame speed for the Cl_2/H_2 system. This work highlights the importance of the validation process when assembling a novel gas-phase mechanism. The revised kinetic mechanism has been associated with a conformal condensed phase decomposition model. An adapted pyrolysis law controls the rate of decomposition. The resulting coupled model has been validated on the case of the low-pressure AP flame studied by Ermolin [5] and Tereshenko [6]. The molar profiles of the main species and the temperature profile obtained are in good agreement with the available experimental data. The macroscopic characteristics of AP combustion (surface temperature, regression velocity) were evaluated at different pressures. The regression velocity shows a pressure dependence of the form aP^n with n decreasing with pressure. This result is consistent with experimental observations and represents a specificity of the new model compared to other reference models. A Zel'dovich-Novozhilov stability study was performed at variable pressure. The model is intrinsically stable up to 11 MPa, allowing for unsteady simulation to be performed over a wide range of operational pressure. The evolution of the temperature sensitivity coefficient agrees with the experimental data.

6. Acknowledgments

The authors would like to thank Direction Générale de l'Armement and ONERA for funding and supporting the present work.

References

[1] A. I. Atwood et al. "Burning rate of solid propellant ingredients, part 1: Pressure and initial temperature effects". In: *Journal of Propulsion and Power* 15.6 (1999), pp. 740–747.

[2] N. N. Bakhman et al. "Investigation of the thermal structure of the burning zone in condensed mixtures by fine thermocouples". In: *Combustion and Flame* 26 (1976), pp. 235–247.

[3] J. Powling. "Experiments relating to the combustion of ammonium perchlorate-based propellants". In: *Symposium (International) on Combustion*. Vol. 11. 1. Elsevier. 1967, pp. 447–456.

[4] O. P. Korobeinichev et al. "Investigation of the structure of a combustion wave of mixed systems based on APC, PMMA, and a catalyst using mass-spectrometric and thermocouple methods". In: *Combustion, Explosion and Shock Waves* 13.3 (1977), pp. 273–279.

[5] N. E. Ermolin et al. "Measurement of the concentration profiles of reacting components and temperature of an ammonium perchlorate flame". In: *Combust., Explos. Shock Waves (Engl. Transl.);(United States)* 18.1 (1982).

[6] A. G. Tereshchenko and O. P. Korobeinichev. "Correctness of mass-spectrometric probe measurements when investigating the flame structure of condensed systems". In: *Combust., Explos. Shock Waves (Engl. Transl.);(United States)* 18.6 (1983).

[7] M. Tanaka and M. Beckstead. "A three-phase combustion model of ammonium perchlorate". In: *32nd Joint propulsion conference and exhibit*. 1996, p. 2888.

[8] Q. Jing, M. Beckstead, and M. Jeppson. "Influence of AP solid-phase decomposition on temperature profile and sensitivity". In: *36th AIAA Aerospace Sciences Meeting and Exhibit*. 1998, p. 448.

[9] N. Meynet. "Simulation numérique de la combustion d'un propergol solide". PhD thesis. Université Paris VI, 2005.

[10] M. L. Gross. "Two-dimensional modeling of AP/HTPB utilizing a vorticity formulation and one-dimensional modeling of AP and ADN". PhD thesis. Brigham Young University, 2007.

[11] D. A. Smyth. "Modeling Solid Propellant Ignition Events". PhD thesis. Brigham Young University, 2011.

[12] K. P. Shrestha et al. "Detailed kinetic mechanism for the oxidation of ammonia including the formation and reduction of nitrogen oxides". In: *Energy & fuels* 32.10 (2018), pp. 10202–10217.

[13] B. V. Novozhilov. “Theory of nonsteady burning and combustion stability of solid propellants by the Zeldovich-Novozhilov method”. In: *Nonsteady burning and combustion stability of solid propellants(A 92-43451 18-28). Washington, DC, American Institute of Aeronautics and Astronautics, Inc., 1992,* (1992), pp. 601–641.

[14] M. D. Smooke et al. “Computational and experimental study of ammonium perchlorate/ethylene counterflow diffusion flames”. In: *Proceedings of the Combustion Institute* 28.2 (2000), pp. 2013–2020.

[15] N. E. Ermolin. “Model for chemical reaction kinetics in perchloric acid-ammonia flames”. In: *Combustion, Explosion and Shock Waves* 31.5 (1995), pp. 555–565.

[16] M. Pelucchi et al. “High-temperature chemistry of HCl and Cl2”. In: *Combustion and Flame* 162.6 (2015), pp. 2693–2704.

[17] O. Mathieu and E. L. Petersen. “Experimental and modeling study on the high-temperature oxidation of Ammonia and related NOx chemistry”. In: *Combustion and flame* 162.3 (2015), pp. 554–570.

[18] A. Hayakawa et al. “Laminar burning velocity and Markstein length of ammonia/air premixed flames at various pressures”. In: *Fuel* 159 (2015), pp. 98–106.

[19] V. F. Zakaznov, L. A. Kursheva, and Z. I. Fedina. “Determination of normal flame velocity and critical diameter of flame extinction in ammonia-air mixture”. In: *Combustion, Explosion and Shock Waves* 14.6 (1978), pp. 710–713.

[20] U. J. Pfahl et al. “Flammability limits, ignition energy, and flame speeds in H2–CH4–NH3–N2O–O2–N2 mixtures”. In: *Combustion and Flame* 123.1-2 (2000), pp. 140–158.

[21] P. D. Ronney. “Effect of chemistry and transport properties on near-limit flames at microgravity”. In: *Combustion Science and Technology* 59.1-3 (1988), pp. 123–141.

[22] T. Jabbour and D. F. Clodic. “Burning Velocity and Refrigerant Flammability Classification”. In: *ASHRAE Transactions* 110 (2004), p. 522.

[23] K. Takizawa et al. “Burning velocity measurements of nitrogen-containing compounds”. In: *Journal of hazardous materials* 155.1-2 (2008), pp. 144–152.

[24] G. Dayma and P. Dagaut. “Effects of air contamination on the combustion of hydrogen—effect of NO and NO2 addition on hydrogen ignition and oxidation kinetics”. In: *Combustion science and technology* 178.10-11 (2006), pp. 1999–2024.

[25] A. Lifshitz and P. Schechner. “The mechanism of the H2+ CL2 reaction: Ignition behind reflected shocks”. In: *International Journal of Chemical Kinetics* 7.1 (1975), pp. 125–142.

[26] J. C. Leylegian, H. Y. Sun, and C. K. Law. “Laminar flame speeds and kinetic modeling of hydrogen/chlorine combustion”. In: *Combustion and flame* 143.3 (2005), pp. 199–210.

[27] R. J. Kee et al. *CHEMKIN-III: A FORTRAN chemical kinetics package for the analysis of gas-phase chemical and plasma kinetics*. May 1996.

[28] A. Ern and V. Giovangigli. *Multicomponent transport algorithms*. Vol. 24. Springer Science & Business Media, 1994.

[29] A. Ern and V. Giovangigli. “Fast and Accurate Multicomponent Transport Property Evaluation”. In: *Journal of Computational Physics* 120.1 (Aug. 1995), pp. 105–116.

[30] L. R. Petzold. “Description of DASSL: a differential/algebraic system solver”. In: (Sept. 1982).

[31] M. W. Chase. “NIST-JANAF thermochemical tables”. In: *J. Phys. Chem. Ref. Data, Monograph* 9 (1998).

[32] D. M. Hanson-Parr and T. P. Parr. “Thermal properties measurements of solid rocket propellant oxidizers and binder materials as a function of temperature”. In: *Journal of energetic materials* 17.1 (1999), pp. 1–48.

[33] T. L. Boggs. “Deflagration rate, surface structure, and subsurface profile of self-deflagrating single crystals of ammonium perchlorate”. In: *AIAA Journal* 8.5 (1970), pp. 867–873.

[34] S. Rahman, V. Giovangigli, and V. Borie. “Pressure and initial temperature sensitivity coefficient calculations in ammonium perchlorate flames”. In: *Journal of Propulsion and power* 27.5 (2011), pp. 1054–1063.

[35] C. Guirao and F. A. Williams. “A model of ammonium perchlorate deflagration between 20 and 100 atm”. In: *AIAA Journal* 9.7 (1971), pp. 1345–1356.

[36] M. R. Denison and E. Baum. “A simplified model of unstable burning in solid propellants”. In: *ARS Journal* 31.8 (1961), pp. 1112–1122.